



HAL
open science

Effect of free-stream turbulence on conical vortex dynamics

Christophe Sicot, Rodolphe Perrin, Faisal Affejee, Jacques Borée

► **To cite this version:**

Christophe Sicot, Rodolphe Perrin, Faisal Affejee, Jacques Borée. Effect of free-stream turbulence on conical vortex dynamics. *International Journal of Heat and Fluid Flow*, 2021, 91, pp.108841. 10.1016/j.ijheatfluidflow.2021.108841 . hal-04093390

HAL Id: hal-04093390

<https://hal.science/hal-04093390>

Submitted on 22 Jul 2024

HAL is a multi-disciplinary open access archive for the deposit and dissemination of scientific research documents, whether they are published or not. The documents may come from teaching and research institutions in France or abroad, or from public or private research centers.

L'archive ouverte pluridisciplinaire **HAL**, est destinée au dépôt et à la diffusion de documents scientifiques de niveau recherche, publiés ou non, émanant des établissements d'enseignement et de recherche français ou étrangers, des laboratoires publics ou privés.



Distributed under a Creative Commons Attribution - NonCommercial 4.0 International License

Effect of free-stream turbulence on conical vortex dynamics

C. Sicot^{a,*}, R. Perrin^{a,b}, F. Affejee^a, J. Borée^a

^a*Institut PPRIME UPR-3346, CNRS - Université de Poitiers - ENSMA, Teleport 2, 1 Avenue Clement Ader, 86360 Chasseneuil-duPoitou, France*

^b*Department of Mechanical Engineering, Faculty of Engineering at Sriracha, Kasetsart University Siracha Campus, Sriracha, Chonburi 20230, Thailand*

Abstract

The influence of Free-Stream Turbulence (FST) on the space-time dynamics of a conical vortex developing along a A-pillar is studied experimentally. Measurements of unsteady wall pressure and velocity by High Speed-Stereo PIV highlight the important effects of turbulence on the mean and instantaneous properties of the vortex. Very significant increases in Reynolds stresses into the vortex region and in wall fluctuating pressure are observed in the presence of FST. In smooth flow, the frequency content of the pressure and velocity fields is very rich with low and high frequency contributions due to the meandering of the vortex and instabilities in the vortex core. Meandering shows, for the different integral length scales and intensities of turbulence tested, a great receptivity to the presence of a FST and we observe a global motion of the vortex structure at low frequency. This frequency is modulated by the value of the integral length scale of the FST. We show that the mean conical structure is a wave guide for the perturbations of the core but that, with FST, the spatio-temporal evolution of the envelope overwhelms the intrinsic instability of the vortex core observed in smooth flow.

Keywords:

Conical vortex, Free-stream Turbulence, A-pillar, velocity-pressure measurements

*Corresponding author

Email address: christophe.sicot@ensma.fr (C. Sicot)

1. Introduction

Conical vortices generated over surfaces having a swept angle with the incident wind are found in a large class of practical applications such as aerodynamics [22], civil engineering [16] and transport engineering [18][12][13]. The study presented in this paper is related to the aerodynamic and aero-acoustic of passenger vehicles and focuses on the A-pillar vortex, arising on the corner edge between the windshield and the front side window. The particularity of this structure is its strong interaction with the lateral wall of the car generating noise inside the cabin [14][3].

The dynamics of this vortex is different from the fully developed vortices evolving without wall interaction (wing-tip and trailing vortices), which are widely studied experimentally, numerically or theoretically in literature ([10], [4], [15], [11], [8], [5] for example). This vortex structure is formed by two vortices, a primary and a secondary one located inside a recirculation zone, generated by the adverse pressure gradient at the wall due to the interaction between the primary vortex and the wall ([19] and [16]). As described by different authors ([12], [4], [15], [16]), the spatio-temporal dynamics of this class of vortex is complex. Unsteady measurements of velocity or wall pressure have shown that the spectra obtained in this type of flow can contain many contributions coming from different sources such as meandering (or wandering), instabilities of the shear layer and/or of the vortex core, or the rotation of the vortex axis. No author, to our knowledge, has clearly identified physical origins to the set of frequency contributions observed in the spectra. All the authors nevertheless agree that meandering appears at a much lower frequency than the other contributions. As the configurations studied are quite different from one author to another, highlighting a universal dimensionless frequency seems complicated. Moreover, not only the temporal characteristics but also the spatial length scales and when possible the determination of the transport properties from a cross-spectral analysis are essential data if one wants to understand the wall fluctuating pressure field.

The main objective of this paper is to analyze the effects of upstream turbulence on the spatio-temporal dynamics of conical vortices and their pressure footprint at the wall. Kawai et al. [16] and Howell et al.[13], using only the wall pressure measurement, have shown that the addition of Free Stream Turbulence (FST) increases significantly the fluctuating pressures at the wall below the vortex. Bailey et al. [4] showed, in the case of a

trailing vortex, a significant increase in meandering motion of the vortex in the presence of FST. However, there is no work which deals with the effect of FST on the spectral content of fluctuating velocity fields and fluctuating wall pressure fields simultaneously.

We propose here a pressure-velocity coupled analysis of the effects of FST. We experimentally studied the flow around a model that generates an A-pillar vortex representative of those encountered on cars. For this purpose, besides a low-turbulence case used for comparisons, two grids are used to generate in the wind tunnel FST with turbulence intensities of 3% and 6%. The flow is analysed using wall pressure measurements and High-Speed PIV. The first section presents the experimental set-up. The second part presents a comparison of the mean and fluctuating properties of the vortex for the smooth flow and the flow with the highest intensity of turbulence. An analysis of the spatio-temporal dynamics of the vortex is finally presented for all the studied flow configurations.

2. Experiments

The experiments were performed in the S120 wind tunnel at ISAE-ENSMA. It is a closed loop wind tunnel with an octogonal test section (1.2 m²). A dihedron has been chosen as an adequate configuration to reproduce the generic feature of the A-pillar vortex flow (figure 1). This kind of model has been used in previous studies for topology description [19] or to test control methods [17]. In order to have a geometry closer to the geometry of a road vehicle, the two lateral sides of the model are inclined at 10° while the angle of the forward facing ramp is 30° [12]. A hoof with an ellipsoidal leading edge was added at the bottom of the model to avoid any risk of separation that would disrupt the dynamics of the vortex. A rough strip, having 20 mm width, (using carborundum of 400 μm height) was positioned across the width of the front side, 5 mm from the nozzle, to trigger a turbulent boundary layer. The free stream velocity is fixed and equal to $U_\infty = 30 \text{ m.s}^{-1}$. The height of the model is $H = 220 \text{ mm}$. The length and the width of the model are equal to $3.67H$ and $1.15H$ respectively. The Reynolds number, based on the square root of the cross section is $Re = 410\,000$. The wind tunnel blockage ratio is 6%. As our motivation was here to minimize interactions with the ground, the body is placed at the center of the test section, supported by three feet, in order to place it outside the boundary layer.

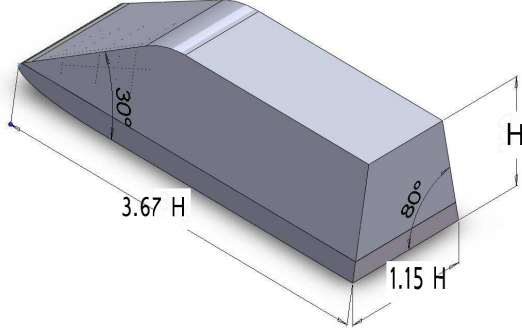


Figure 1: Geometry and dimensions of the model

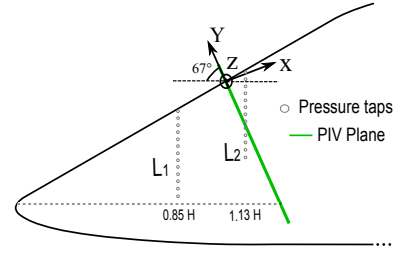


Figure 2: Pressure taps and PIV plane position

Table 1: Turbulence generated at the nose of the model

	$Tu3\%$	$Tu6\%$
Intensity (%)	2.7	6.4
Integral length scale (L/H)	0.06	0.12

Without any added setup, the free stream turbulence level in the test section is less than 0.2% at the body location. Higher turbulence levels have been classically generated in the test section using two square-mesh perforated plates (grids) mounted at the entrance of the test section (1.2m upstream of the nose of the model) [9]. The small grid had a mesh size $M = 40$ mm, whereas the large grid had $M = 120$ mm. The results obtained in the presence of these two grids will be named $Tu3\%$ and $Tu6\%$ respectively in this paper. To characterize the free-stream conditions generated by each grid, three-component velocity measurements, using hot wire, of the grid turbulence were performed with the model removed from the wind tunnel. The characteristics of the generated turbulences at a longitudinal position corresponding to the position of the nose of the model are reported in the table 1. Further details on the turbulence generated can be found in the work of Affeje [1].

High-Speed Stereo Particle Image Velocimetry (HS-SPIV) was used to obtain the three components of the velocity field at a frequency of 4 kHz in a plane located at a distance from the front of the model of $1.13H$ (figure 2). The laser sheet was positioned with a 23° angle with the vertical

axis so that the plane is perpendicular to the time-averaged axis of development of the vortex (the A-pillar vortex axis was previously identified to be inclined at an angle of 23° with the horizontal axis [2]). Illumination was provided by a Quantronix-527-30 laser emitting two pulses of 18 mJ (laser sheet thickness ≤ 1 mm). An oil generator has provided seeding with a mean particles diameter of about $1 \mu\text{m}$. 24 000 velocity fields were acquired for each configuration with two Photron Fastcam SA1.1 camera. The resolution of the sensor is 832×736 px². A multipass algorithm with a final interrogation window size of 16×16 px² and 50% overlapping was applied. The final size of the interrogation window was 1.7 mm x 1.7 mm. The time interval between two laser shots was fixed at 20 μs . The maximum uncertainty on instantaneous velocity measurements has been estimated at $0.56 \text{ m}\cdot\text{s}^{-1}$ (displacement of 0.1 pixel). The flow will be described henceforth using a cartesian coordinate system (X, Y, Z) related to the PIV-plane to indicate the axial, vertical and transverse directions (figure 2). All quantities are made dimensionless using the height of the model H and the free stream velocity U_∞ . The components of the mean and instantaneous velocity field are denoted respectively by $(\bar{U}, \bar{V}, \bar{W})$ and (U, V, W) . The components of the instantaneous fluctuating velocity field are denoted respectively by (u, v, w) .

Wall pressure measurements have also been carried out on the side of the model. Figure 2 presents the position of the pressure taps located in two vertical lines L_1 and L_2 . The measurements of the wall fluctuating pressure have been obtained with off-set sensors because the distance between pressure holes can be much smaller than the one achieved with flush mounted sensors. Those sensors are differential and have a pressure range of 250 Pa. For each probe, the frequency response has been measured (magnitude and phase) with a specially designed coupler and a reference microphone (see Ruiz et al.[23] for more details about pressure sensors calibration). The signal recorder is able to simultaneously acquire 30 pressure probe signals with an effective sampling frequency of 6.25 kHz and a cut-off frequency of the anti-aliasing filters set at 2 kHz. For each measurement, the acquisition duration was 120 s. For the spectral analysis, the modified periodogram method of Welch has been used, each time series being split into segments of 4096 points with a 50% overlap.

3. Mean and fluctuating properties

In this section, the purpose is to analyse usual first and second order statistical moments of the velocity and the wall pressure in order to detect the main effect of external turbulence. For the sake of brevity, only smooth flow and $Tu6\%$ data are presented. Figure 3 presents isocontours of the mean vorticity component normal to the measurement plane. The vortex structure is composed of two regions with high vorticity: the shear layer and the primary vortex. Previous studies (Levy et al. [19] for example) highlighted the presence of a counter-rotating secondary vortex located inside the recirculation zone and generated by the adverse pressure gradient at the wall due to the interaction between the primary vortex and the wall. The resolution of our measurements is not sufficient here to observe this secondary vortex, probably located in the region near the wall at $Y \approx -0.05$. Indeed, from the measurements of Levy [19], we can estimate that the diameter of this secondary vortex is about 2 mm at the scale of our experiment which is here about the PIV resolution. Concerning the addition of upstream turbulence, as observed by Bailey [4] for a wing-tip vortex, it has a very weak effect on mean vortex size and average position. We can nevertheless observe a decrease in the mean vorticity in the whole vortex structure.

More quantitatively, figures 4 and 5 present mean vorticity and velocity profiles along a horizontal line passing through the mean core of the primary vortex (dotted line on figure 3). **The value of vorticity is clearly lower in the core of the vortex in turbulent flow possibly due to the increase of the mean turbulent transport of momentum inside the structure and/or a more intense meandering of the structure.** In the remainder of the paper, the separated analysis of the dynamics of the shear layer and of the primary vortex will clarify the link between the influence of upstream turbulence on vorticity field and the increase in meandering motion of the vortex.

As observed on the vorticity maps, the position of the vortex center, defined as the location where $\overline{V} = \overline{W} = 0$, is not affected by the freestream turbulence. **At this point ($Z \approx 0.085$), it is interesting to note that the mean axial velocity is lower than the upstream velocity ($U_{core} \approx 0.8.U_\infty$) in agreement with Hoarau [12] and Levy [18]. We also point out here that the addition of external turbulence has no influence on this mean axial velocity at the core of the vortex.**

Reynolds stresses are presented in figure 6. In smooth flow, whatever the component, we observe a local maximum at the position of the vortex

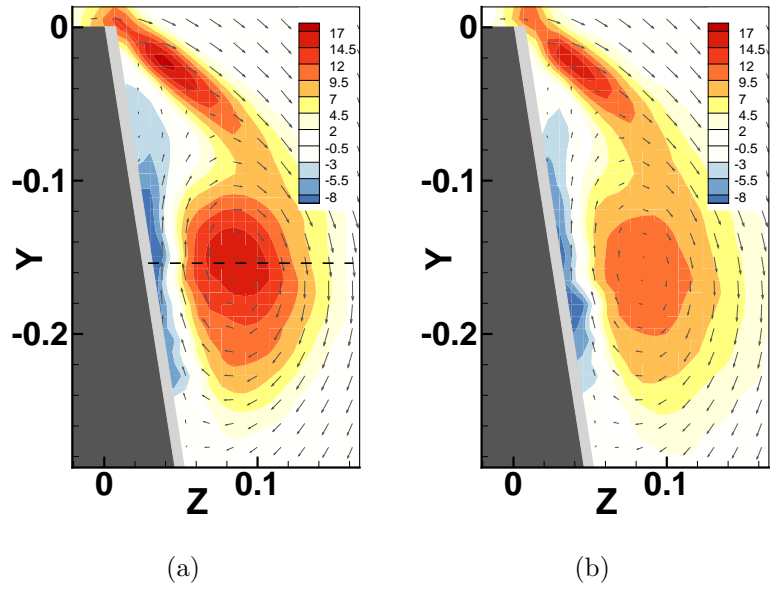


Figure 3: Mean vorticity fields. Left : Smooth flow ; Right : $Tu6\%$. Only one in two vectors is shown for clarity

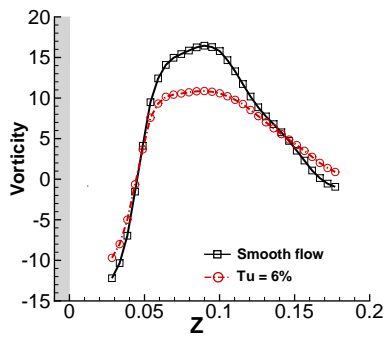


Figure 4: Vorticity profiles along a horizontal line passing through the mean core of the vortex ($Y = -0.15$)

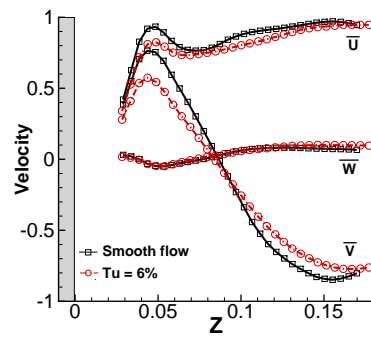


Figure 5: Mean velocity profiles along a horizontal line passing through the mean core of the vortex ($Y = -0.15$)

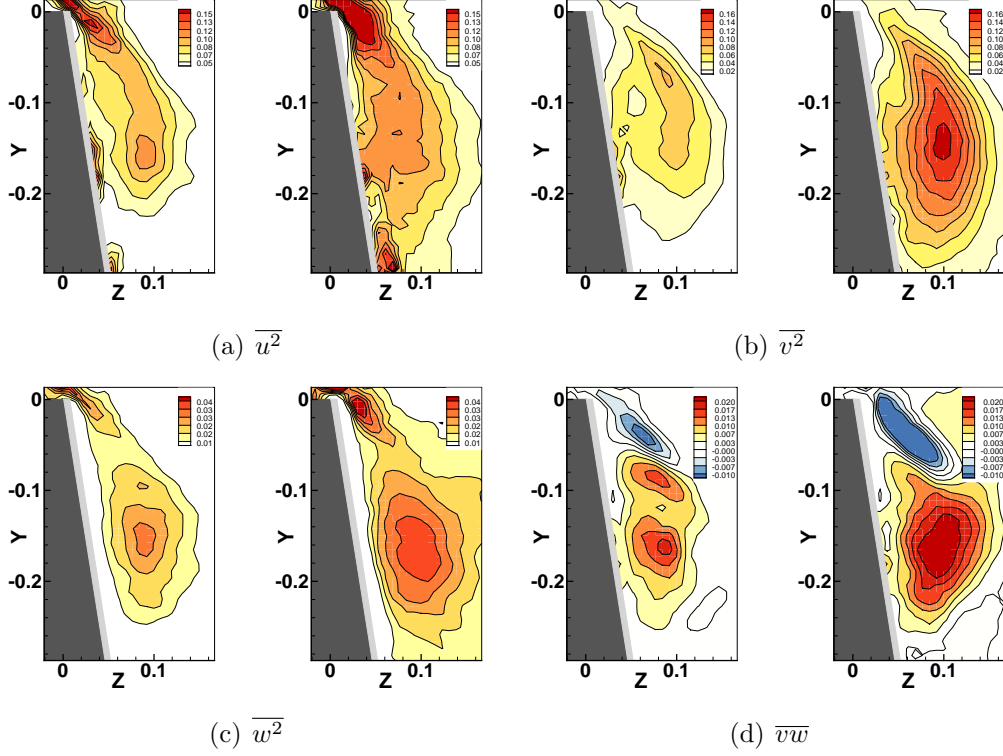


Figure 6: Reynolds stresses. For each figure: Left : Smooth flow ; Right : $Tu6\%$

core ($(Y_v, Z_v) \approx (-0.15, 0.085)$). The contributions $\overline{u^2}$ et $\overline{w^2}$ also have local maxima in the shear layer near the separation. The \overline{vw} distribution presents three local extrema: (i) **one in the shear layer where $\overline{vw} < 0$ due to the downward transport of the fluctuating lateral and longitudinal momentum by the fluctuating vertical motion in the turbulent shear layer**, (ii) one located at $Y \approx -0.1$ probably linked to the interaction between the primary vortex and the incoming vorticity sheet and (iii) one near the vortex core ($Y \approx -0.15$). Whatever the contribution, a significant increase of the turbulent kinetic energy in the structure is observed in turbulent flow. In particular, the value of the contribution $\overline{v^2}$ is doubled at the vortex core. Bailey et al. [4] have made similar observations for a wing tip vortex and linked this increase of turbulent kinetic energy to the high receptivity of the meandering of the vortex to the external turbulence.

Concerning the effect of FST on the wall pressure, figures 7 and 8 present the mean and fluctuating pressure coefficient, $C_p = (p - p_\infty)/(\frac{1}{2}\rho U_\infty^2)$ and

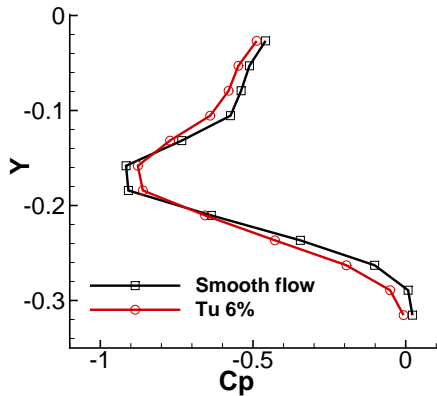


Figure 7: Mean wall pressure coefficient

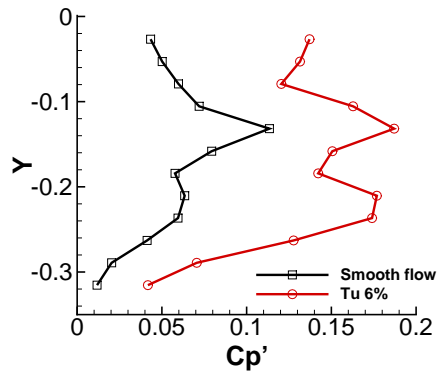


Figure 8: Fluctuating wall pressure coefficient

$$C'_p = \sqrt{p'^2} / (\frac{1}{2}\rho U_\infty^2) \text{ on the line } L_2.$$

The mean pressure profile shows that the position of the time-averaged vortex core, associated with a low pressure level at $Y \approx -0.15$, is not affected by the FST whereas a decrease of the value of the pressure gradient on each side of this low pressure region is observed.

Concerning the fluctuating pressure, two maxima are observed in smooth flow at $Y \approx -0.13$ and $Y \approx -0.22$. These maxima, whose positions correspond to the location of the extrema of the mean pressure gradients, are due to the spatial fluctuation of the structure. As the highest maxima ($Y \approx -0.13$) is close to the secondary separation point (estimated from the velocity field) the high level of fluctuations at this point, seems generated by the combined effects of the motion of the structure and by the spatial fluctuation of the secondary separation point. **In turbulent flow, there is an important and overall increase of C'_p (multiplied by 2), even for pressure sensors located just below the edge of the model ($Y \geq -0.1$) and the two peaks have the same amplitude.** This suggests that in presence of FST, the overall motion of the vortex is responsible for this significant increase. We will see in the next section that this hypothesis will be largely reinforced by the study of the spatio-temporal properties of the flow.

4. Spatio-temporal properties

One point statistics discussed above are not sufficient to understand the spatio-temporal properties of the conical vortex. For this reason, we

present in this section spatial correlations of integral quantities and spectral content of the pressure and velocity fields.

In a first step, the instantaneous raw velocity fields were filtered using Proper Orthogonal Decomposition [20]. The POD direct method has been applied to the three components of the velocity, and a decomposition of the form:

$$U_i(P, t) = \bar{U}_i(P) + \sum_n a_n(t) \Phi_i^{(n)}(P)$$

was classically obtained for each dataset, where a_n are the temporal coefficients, and Φ^n are the modes which depend on $P = (Z, Y)$. A previous study presented by Affejee et al. [2] has shown that it is sufficient to keep the first 10 calculated POD modes to reconstruct the velocity field. Indeed, systematic tests have shown a negligible influence of the increase in the number of modes considered on the vortex characteristics.

Figure 9 shows an example of a comparison between a raw instantaneous vorticity field and one reconstructed using the 10 most energetic POD modes. One can see that small scales are well filtered out by POD and that the larger scales are well reproduced. From these reconstructed fields, we define the primary vortex as the region where the vorticity, Ω_x , is greater than a threshold value. An example of a contour (in dotted line) is shown in figure 9 (center) for a threshold value $\Omega_x = 2$. Systematic tests have shown that the choice of this threshold value has very little influence on the flow dynamics analyzed in the following [1].

As previously described, it can be seen from the figure 9 that the vortex consists of two regions which can be separated: the shear layer and the primary vortex. The objective of this part is to analyze the spatio-temporal dynamics of these two regions first separately then in a coupled way. For that, we have to spatially separate these two areas. The region delimited by $\Omega_x > 2$ has been cut off at the value $y = y_s$ where a saddle point was detected in the vorticity fields. **To locate the saddle point in one instantaneous field, the maximum of Ω_x is first calculated on every horizontal line in the field and then the location of the minimum value of those maximum values gives the location y_s of the saddle point.**

The primary vortex is then defined as the region where $\Omega_x > 2$ and $y < y_s$ (figure 9 (right)) and the center of the primary vortex (Z_v, Y_v) is then determined as the barycenter based on the vorticity in this region. As this was done for every instantaneous field, this allowed to follow the instantaneous characteristics of the vortex (size, center, etc...). **We checked that others**

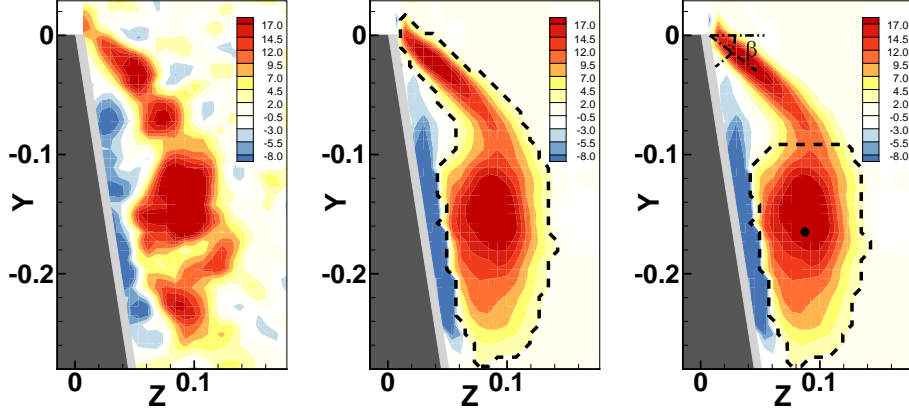


Figure 9: Instantaneous vorticity field. Left: Raw field ; Center: Field reconstructed with a 10 POD mode filtering ; Right: Definition of primary vortex region and shear layer angle

vortex identification criteria (Q criterion, λ , ...) give very similar results for the vortex region. However, it would not be possible to analyse the dynamics of the shear layer using such criterium. In order to keep the analysis based on a same quantity, we therefore have chosen to use vorticity in what follows.

In order to follow the temporal dynamics of the shear layer, the angle beta (see Figure 9 (right)) is defined as the angle (with respect to the horizontal) at which the maximum of vorticity is found on an circular arc of radius $r = 0.063$ about the corner point (independency of the shape of the Probability Density Function of β with respect to r has been checked in the range $0.063 < r < 0.086$).

We now present the results obtained from the analysis of the instantaneous fields filtered by POD. First, the spatial dynamics are analysed by considering the Probability Density functions (PDF) of different characteristics of the vortex motion (core position (Z_v, Y_v) , size of the primary vortex (Σ) and separation angle of the shear layer (β)) and spatial correlations of velocity and pressure. In a second time, the temporal dynamics will be analyzed through the study of the pressure and velocity Power Spectral Density (PSD) at different points in the flow and on the wall and through the study of different coherence functions.

Figure 10 presents the Probability Density Function (PDF) of the position of the vortex core obtained from instantaneous fields. The arrow represents the preferred direction of the vortex core motion obtained as the eigenvector

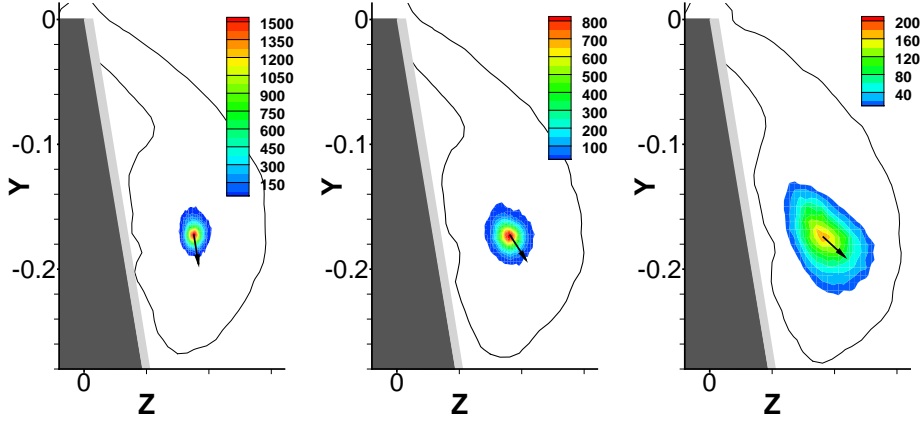


Figure 10: Probability Density Function of the primary vortex center (color). Isocontour of vorticity $\Omega_x = 2$ (line). Smooth flow (left). $Tu3\%$ (middle). $Tu6\%$ (right)

associated with the highest eigenvalue of the covariance matrix :

$$\begin{pmatrix} \overline{(Z'_v)^2} & \overline{Z'_v Y'_v} \\ \overline{Z'_v Y'_v} & \overline{(Y'_v)^2} \end{pmatrix}$$

While the most probable position of the vortex core is not modified by the presence of a turbulent flow upstream, we observe here that the turbulence significantly increases the displacement of this core. This is in good agreement with what has been observed on one point statistics. In addition, while the preferred direction of displacement of the core is almost parallel to the lateral wall for a flow without turbulence, it is strongly inclined (approximately 45°) for the other two turbulence intensities. This result is consistent with the large increase in Reynolds stress, \overline{vw} , observed previously (figure 6).

Figure 11 shows the Probability Density Function of the orientation of the shear layer (β) and the size of the vortex (Σ).

We can notice first of all that while the intensity of turbulence has a very weak effect on the mean separation angle of the shear layer, the time-averaged size of the vortex increases with the intensity and the integral scale of the upstream turbulence. We can also observe that the Probability Density Functions are wider and have a different shape when the turbulent intensity increases. It can be noted that while being intermediate between the narrow smooth flow PDF and the wide $Tu6\%$ PDF, the $Tu3\%$ PDF is fairly close

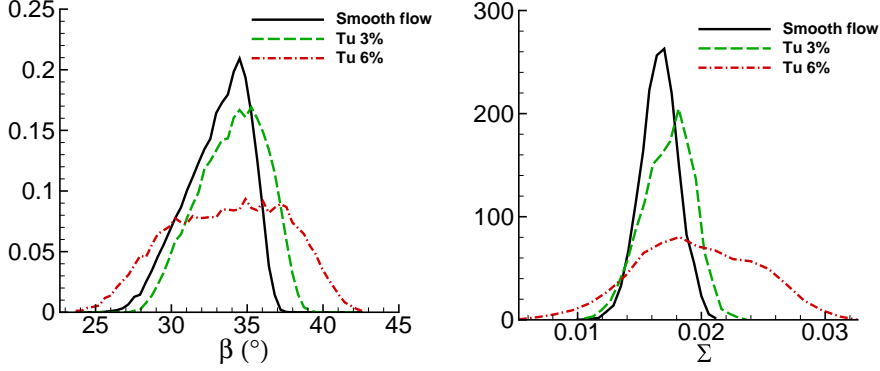


Figure 11: Probability Density function of angle of the shear layer (left) and size of the primary vortex (right)

in shape to that obtained without FST. We believe that this is due to a greater interaction of the upstream turbulence with the vortex in the $Tu6\%$ configuration because in this situation the integral scale of the turbulence is very close to the characteristic length of the vortex (its diameter here). This superposition of scale then leads to a great receptivity of the vortex structure to external perturbations [6].

The spatio-temporal analysis presented at the end of this section will confirm the global response of the conical vortex to the external turbulence and the corresponding low frequency modulation of its physical properties (see e.g. figures 16 and 17). The power spectral density of the angle β , not shown here for brevity, confirms that the increase of the variance of β observed in figure 11 is indeed due to such a low frequency modulation. We may then assume that the PDF of β results from the combination of the unsteadiness of the 3D separation driven by the 3D shear layer, modulated by low frequency perturbations due to the external turbulence. A systematic study varying not only the turbulence intensity but also the integral length scales of the external velocity field is therefore needed to determine the range of angle modulated by external turbulence.

The global dynamics of the structure is also highlighted by the study of the spatial correlations of velocity and pressure. The spatial velocity correlation, for the vertical component V , is defined as : $R_{vv}(Y_r, Z_r, Y, Z) = \frac{\langle v(Y_r, Z_r) \cdot v(Y, Z) \rangle}{\sqrt{\langle v(Y_r, Z_r)^2 \rangle} \cdot \sqrt{\langle v(Y, Z)^2 \rangle}}$ where (Y_r, Z_r) is the reference point located at the mean vortex core position. The spatial pressure correlation is defined as: $R_{p'p'}(Y_r, Y) =$

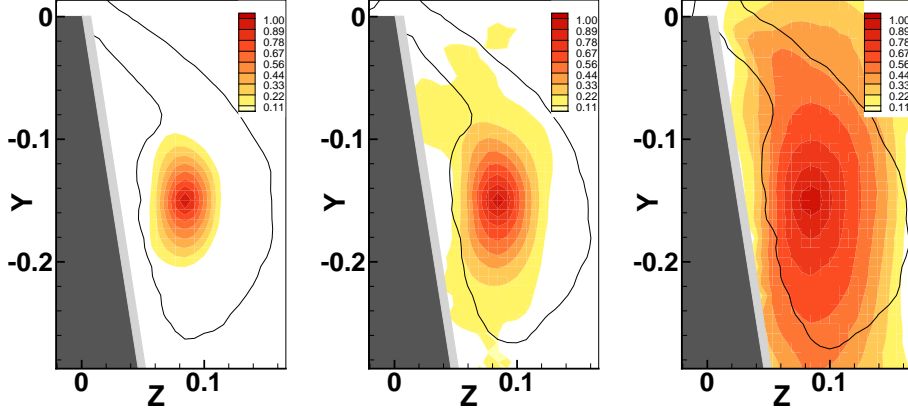


Figure 12: Spatial correlation of the vertical velocity component V (color). The reference point is located at the primary vortex center. Smooth flow (left). $Tu3\%$ (center). $Tu6\%$ (right)

$\frac{\langle p'(Y_r).p'(Y) \rangle}{\sqrt{\langle p'(Y_r)^2 \rangle}.\sqrt{\langle p'(Y)^2 \rangle}}$ where the chosen reference point, $Y_r = -0.24$, corresponds to the position of the primary vortex reattachment point obtained from oil flow visualisations [1].

Regarding the spatial correlation of velocity (figure 12), in smooth flow, significant levels of correlations are restricted to a very limited region near the vortex core. The correlation is very low in the shear layer region, suggesting that, in this plane, the meandering of the primary vortex is not correlated with the dynamics of the shear layer. As on the probability density function previously presented, we can notice that the correlation obtained in the configuration $Tu3\%$ is quite close to that obtained without upstream turbulence whereas in the $Tu6\%$ configuration, a significant correlation exists between the vertical velocities at the core of the vortex and in the shear layer, suggesting an overall response of the vortex dynamics leading to a large scale displacement.

These analyses are reinforced by the distribution of spatial pressure correlation (figure 13). Indeed, for the smooth flow case, there is no correlation between the mean reattachment zone and the region just below the shear layer ($Y \geq -0.1$). The lack of correlation between these two zones of the flow confirms that the dynamics of the primary vortex and of the shear layer are not correlated. In contrast, significant levels of correlation are observed in the region $Y > -0.1$ for turbulent flows. This increase in the two-point

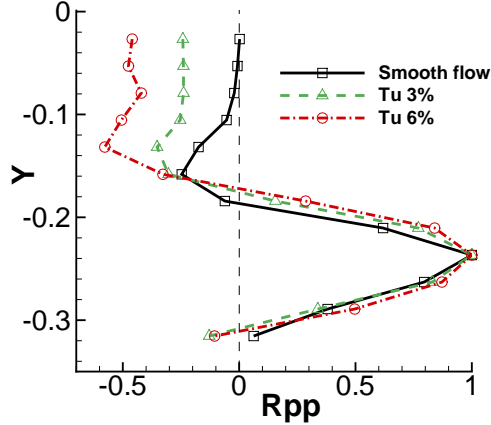


Figure 13: Spatial pressure correlation along the L_2 line. The reference point is located at the mean reattachment point of the primary vortex

pressure correlation between the wall region just below the shear layer and the rest of the structure is the sign of a global motion of the structure.

We are now interested in the temporal dynamics of the flow through the analysis of Power Spectral Densities (PSD). Spectra are plotted against the dimensionless number $St = \frac{f \cdot H}{U_\infty}$. Figure 14 presents velocity spectra for the vertical component (V) obtained at the center of the mean primary vortex.

A wide band contribution ($St \in [3 - 7]$) is clearly visible in smooth flow. We can distinguish two contributions which emerge weakly at $St \approx 3.5$ and $St \approx 5$ (these contributions are reinforced in the $Tu3\%$ configuration). As proposed by Bailey [4] and Kawai [16], these contributions, which are only obvious for not or slightly turbulent configurations, may be associated with instabilities of the vortex core or with a spiral axis rotation of the vortex. The increase in upstream turbulence ($Tu3\%$ configuration) leads to the emergence of a clear low frequency contribution at $St \approx 2$, not observed in the smooth flow configuration, associated with the vortex meandering. The higher frequency contributions, which are still present in the 'intermediate' configuration $Tu3\%$ are no longer distinguished when the upstream turbulence increases while the contribution of meandering becomes even more energetic.

This analysis is reinforced by the study of pressure spectra presented in figure 15. In order to facilitate the understanding of physical phenomena, PSD of pressure are presented only at two characteristic points of the flow:

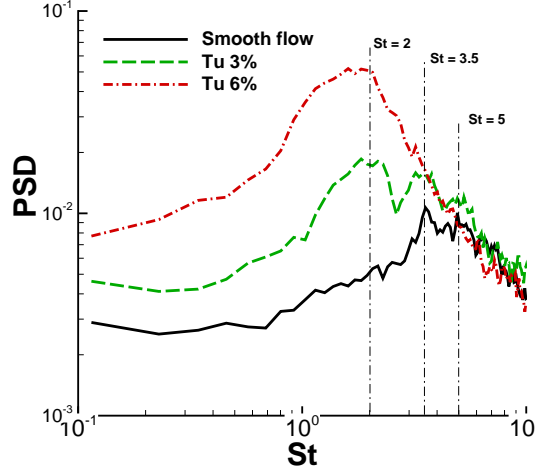


Figure 14: Power Spectral Density of fluctuating velocity (V component) at the mean position of the primary vortex center

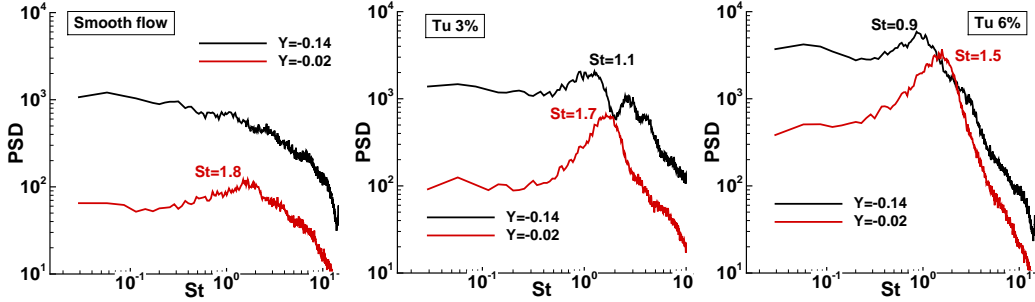


Figure 15: Power Spectral Density of fluctuating pressure along the line L_2 just below the shear layer ($Y = -0.02$) and near the vortex core ($Y = -0.14$).

One near the pillar just under the shear layer ($Y = -0.02$) and one near the vortex core ($Y = -0.14$)

Whatever the position on the wall, the low frequency contribution associated with vortex meandering increases strongly with upstream turbulence. This increase is very significant under the shear layer at $Y = -0.02$ and the power spectral densities in the frequency band of meandering are similar at both positions with FST. A decrease of the meandering peak frequency when moving away from the pillar is observed (see figure 15). This observation is reinforced by the analysis of all pressure spectra obtained with FST (not presented here for brevity). Near the pillar, just under the shear layer at

$Y=-0.02$, we may expect pressure fluctuations to be due to a spatio-temporal motion of the external envelope (see also figure 16). At $Y=-0.14$, the pressure fluctuation combines the global motion of the envelope and the vortex core dynamics under the forcing of turbulence. Volumetric data would be needed to fully understand the modulation of the peak frequency. **Figure 15** also shows that the peak frequency at both $Y=-0.02$ and -0.14 is slightly lower for $Tu6\%$ than for $Tu3\%$. This modulation is probably dependent on the scale ratio between the characteristic length of the vortex and the integral length scale of the upstream turbulence.

This global response of the conical vortex to the external turbulence is further illustrated when computing **the coherence function [7] between the shear layer angle, β and primary vortex size, Σ (figure 16)**. Indeed, the coherence between these two quantities is really low in smooth flow, in particular at the meandering frequency ($St < 3$), showing an uncorrelated motion of the shear layer and the primary vortex. Conversely, the coherence, at the meandering frequency, is very high in the presence of upstream turbulence. Moreover, the analysis of the phase between these two signals in this band of frequency (not presented here) shows that they evolve in phase opposition. The great receptivity of the meandering to FST then leads to a simpler flow dynamics than in smooth flow. It consists of an overall vortex respiration linked to an increase in the size of the vortex when the angle of the shear layer decreases.

These analyses carried out in the PIV plane are supported by cross-spectrum along the mean vortex core. The spatial coherence and phase between pressure signals measured on the two lines L1 and L2 is displayed on figure 17. For the sake of clarity, we have chosen to present the results obtained at the main reattachment point which are representative of all the data analyzed.

For smooth flow, the coherence values are weak. A maximum of 30% is reached in the frequency band associated previously to the vortex core instabilities ($St=[3-5]$). The coherence values in this frequency band decrease very quickly with the intensity of turbulence while the low frequency contribution ($St < 2$) increases strongly. This contribution, associated with the vortex meandering, not clearly detected without turbulence, becomes very consistent (between 70% and 100% of coherence) in presence of FST. This highlights the large-scale longitudinal dynamics of this oscillating motion.

Considering the phase evolution, we observe, for every FST, a linear evolution in the frequency range where the coherence values are greater than

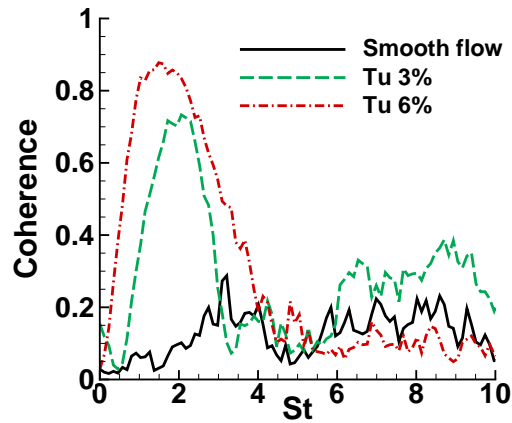


Figure 16: Coherence function between the size of the primary vortex and the shear layer angle

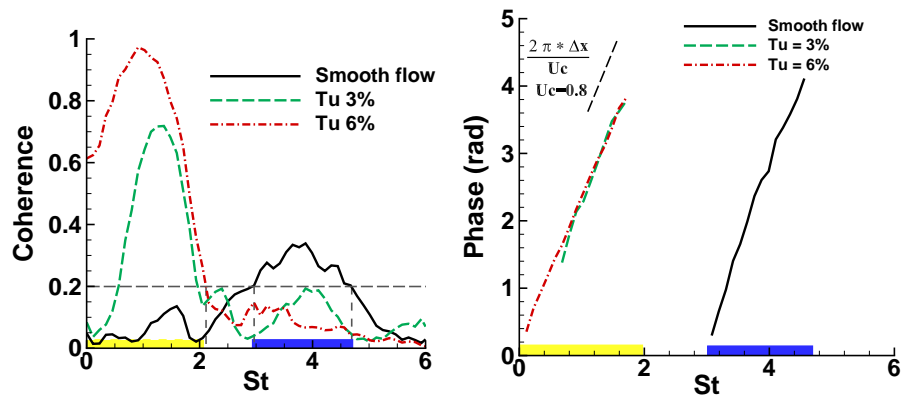


Figure 17: Left : Wall pressure coherence function at the mean reattachment point between the lines L_1 and L_2 . Right : Phase evolution in the frequency domain restricted to the domain where the coherence is larger than 0.2 (dashed line on the left figure). The yellow and blue rectangles correspond to the Strouhal values for which the coherence is greater than 0.2.

0.2. For perturbations transported by the velocity field at a constant mean velocity U_c , the phase difference $d\phi$ depends linearly on the frequency with $\frac{d\phi}{dSt} = 2\pi \cdot \frac{\Delta x}{U_c}$ where Δx is the longitudinal distance between the two pressure taps. The slope of the dashed line drawn in figure 17 (right) has been computed by assuming that perturbations are transported at the velocity $U_c = 0.8$. This velocity was chosen because it corresponds to the axial velocity measured at the mean vortex core (figure 5). A very good agreement is observed between the slope obtained by this simplified model and the slopes of the phase evolutions measured.

For configurations with FST, this linearity of the phase is observed at the low meandering frequency. It is expected that the large scale meandering of the envelope of the vortex results in a large scale deformation of the vortex core that travels downstream at the mean velocity $0.8U_\infty$. The mean conical structure is therefore still a wave guide for the perturbations of the core but the spatio-temporal evolution of the envelope overwhelms the intrinsic instability of the vortex core observed without FST.

5. Conclusions and perspectives

The effects of Free Stream Turbulence on a conical vortex structure were studied by combining Stereo-HS-PIV and multi-point pressure measurements. The dynamics of this vortex in strong interaction with the wall is mainly controlled, for a smooth flow, by instabilities present in the core of the vortex and by an oscillating motion, at lower frequency, called meandering or wandering according to the authors. It has been shown that the time-averaged characteristics of the vortex (size, position) are not affected by the presence of turbulent upstream flow.

Nevertheless, we observe a significant increase in the velocity and wall pressure fluctuations with the intensity of turbulence mainly due to the very significant increase of the meandering motion. This low frequency oscillation leads to a significant dispersion of the instantaneous characteristics of the vortex (size, angle of the separated shear layer). The overall dynamics of the vortex structure is then mainly driven by this multi-scale oscillating motion. The space-time analysis of the wall pressure footprint shows that the mean conical structure is a wave guide for the perturbations of the core but that, with FST, the spatio-temporal evolution of the envelope overwhelms the intrinsic instability of the vortex core observed without FST. Moreover, a modulation of the meandering frequency has been observed as a function of

the position, which suggests an oscillation with deformation of the vortex by the action of FST, as opposed to a 'rigid body like' oscillation. The analysis of velocity and pressure spectra highlighted the frequency modulation of oscillation motion introduced by upstream turbulence. This modulation is probably driven by the ratio between the size of the vortex and the integral length scale of the turbulence.

The comprehension of the influence of upstream turbulence on this unsteady aerodynamic may be viewed as a necessary step to develop control strategies adapted to the nature of the upstream flow enabling real-time adaptation of control strategies to the conditions of use. To do this, it will be necessary to complete the analyses by studying the vortex dynamics subjected to other intensity and length scale of turbulence to understand more finely the respective roles of each.

Acknowledgements

The authors would like to warmly thank F. Paillé, P. Braud and M. Rossard for support during the experiments. We are indebted to the CPER Feder programme Transport for financial support.

References

- [1] Affejee, F. (2015). Analyse physique d'écoulements décollés fortement tridimensionnels par expérimentation. Structuration spatio-temporelle et sensibilité à une turbulence amont (Doctoral dissertation).
- [2] Affejee, F., Sicot, C., Perrin, R. and Borée, J. (2013). Upstream turbulence effects in the spatio-temporal characteristics of a model A-pillar vortex. In Eighth International Symposium on Turbulence and Shear Flow Phenomena. Begel House Inc.
- [3] Alam, F., Watkins, S. and Zimmer, G. (2003). Mean and time-varying flow measurements on the surface of a family of idealised road vehicles. *Experimental thermal and fluid science*, 27(5), 639-654.
- [4] Bailey, S. C. C. and Tavoularis, S. (2008). Measurements of the velocity field of a wing-tip vortex, wandering in grid turbulence. *Journal of Fluid Mechanics*, 601, 281.

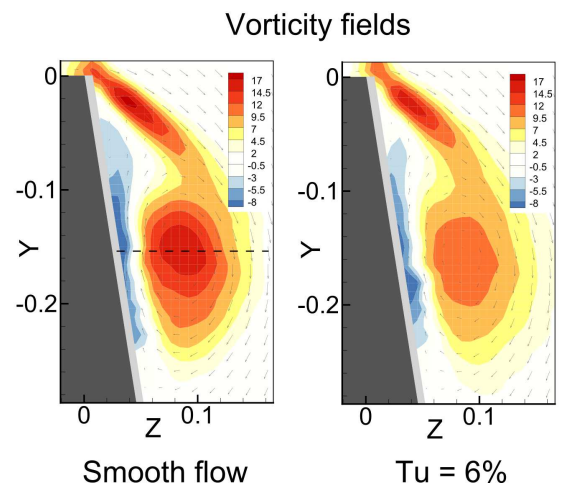
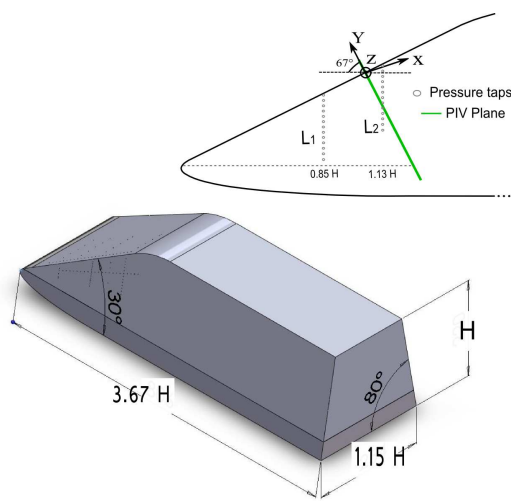
- [5] Bailey, S. C., Pentelow, S., Ghimire, H. C., Estejab, B., Green, M. A. and Tavoularis, S. (2018). Experimental investigation of the scaling of vortex wandering in turbulent surroundings. *Journal of Fluid Mechanics*, 843, 722.
- [6] Bearman, P. W. and Morel, T. (1983). Effect of free stream turbulence on the flow around bluff bodies. *Progress in aerospace sciences*, 20(2-3), 97-123.
- [7] Bendat, J. S. and Piersol, A. G. (1980). *Engineering applications of correlation and spectral analysis*. New York
- [8] Bölle, T., Brion, V., Robinet, J. C., Sipp, D. and Jacquin, L. (2021). On the linear receptivity of trailing vortices. *Journal of Fluid Mechanics*, 908.
- [9] Comte-Bellot, G. and Corrsin, S. (1966). The use of a contraction to improve the isotropy of grid-generated turbulence. *Journal of fluid mechanics*, 25(4), 657-682.
- [10] Devenport, W. J., Rife, M. C., Liapis, S. I. and Follin, G. J. (1996). The structure and development of a wing-tip vortex. *Journal of fluid mechanics*, 312, 67-106.
- [11] Edstrand, A. M., Davis, T. B., Schmid, P. J., Taira, K. and Cattafesta, L. N. (2016). On the mechanism of trailing vortex wandering. *Journal of Fluid Mechanics*, 801.
- [12] Hoarau, C., Borée, J., Laumonier, J. and Gervais, Y. (2008). Unsteady wall pressure field of a model A-pillar conical vortex. *International Journal of Heat and Fluid Flow*, 29(3), 812-819.
- [13] Howell, J., Fuller, J. B. and Passmore, M. (2009). The effect of free stream turbulence on A-pillar airflow (No. 2009-01-0003). SAE Technical Paper.
- [14] Hucho, W. H. and Ahmed, S. R. *Aerodynamics of road vehicles: from fluid mechanics to vehicle engineering*. 1987.
- [15] Jacquin, L. and Pantano, C. (2002). On the persistence of trailing vortices. *Journal of Fluid Mechanics*, 471, 159

- [16] Kawai, H. and Nishimura, G. (1996). Characteristics of fluctuating suction and conical vortices on a flat roof in oblique flow. *Journal of wind engineering and industrial aerodynamics*, 60, 211-225.
- [17] Lehugeur, B., Gilliéron, P. and Kourta, A. (2010). Experimental investigation on longitudinal vortex control over a dihedral bluff body. *Experiments in fluids*, 48(1), 33-48.
- [18] Levy, B. (2009). Analyse et controle de l'écoulement de montant de baie (Doctoral dissertation, Universit de Toulouse, Universit Toulouse III-Paul Sabatier).
- [19] Levy, B. and Brancher, P. (2013). Topology and dynamics of the A-pillar vortex. *Physics of Fluids*, 25(3), 037102.
- [20] Lumley, J. L. (1967). The structure of inhomogeneous turbulent flows. *Atmospheric turbulence and radio wave propagation*.
- [21] Mitchell, A. M. (2000). Caractérisation et contrôle de l'éclatement tourbillonnaire sur une aile delta aux hautes incidences (Doctoral dissertation, Paris 6).
- [22] Mitchell, A. M., Morton, S. A., Forsythe, J. R. and Cummings, R. M. (2006). Analysis of delta-wing vortical substructures using detached-eddy simulation. *AIAA journal*, 44(5), 964-972.
- [23] Ruiz, T., Sicot, C., Brizzi, L. E., Laumonier, J., Borée, J. and Gervais, Y. (2009). Unsteady near wake of a flat disk normal to a wall. *Experiments in fluids*, 47(4-5), 637.
- [24] Saunders, J. W. and Mansour, R. B. (2000). On-road and wind tunnel turbulence and its measurement using a four-hole dynamic probe ahead of several cars. *SAE transactions*, 477-496.

Graphical Abstract

Effect of free-stream turbulence on conical vortex dynamics

C. Sicot, R. Perrin, F. Affejee, J. Borée



Highlights

Effect of free-stream turbulence on conical vortex dynamics

C. Sicot, R. Perrin, F. Affejee, J. Borée

- Influence of upstream turbulence on the spatio-temporal dynamics of a conical vortex
- Experimental measurements using High Speed Stereo PIV and unsteady pressure sensors
- Analysis of spatial and temporal correlations of velocity and wall pressure
- High receptivity of vortex meandering to Free Stream Turbulence
- Modulation of the meandering frequency by Free Stream Turbulence